Lecture Notes in Mechanical Engineering

Krishna Mohan Singh
Sushanta Dutta
Sudhakar Subudhi
Nikhil Kumar Singh *Editors*

Fluid Mechanics and Fluid Power, Volume 1

Select Proceedings of FMFP 2022

Springer

Lecture Notes in Mechanical Engineering

Lecture Notes in Mechanical Engineering (LNME) publishes the latest developments in Mechanical Engineering—quickly, informally and with high quality. Original research reported in proceedings and post-proceedings represents the core of LNME. Volumes published in LNME embrace all aspects, subfields and new challenges of mechanical engineering.

To submit a proposal or request further information, please contact the Springer Editor of your location:

Europe, USA, Africa: Leontina Di Cecco at Leontina.dicecco@springer.com
China: Ella Zhang at ella.zhang@springer.com
India: Priya Vyas at priya.vyas@springer.com
Rest of Asia, Australia, New Zealand: Swati Meherishi
at swati.meherishi@springer.com

Topics in the series include:

- Engineering Design
- Machinery and Machine Elements
- Mechanical Structures and Stress Analysis
- Automotive Engineering
- Engine Technology
- Aerospace Technology and Astronautics
- Nanotechnology and Microengineering
- Control, Robotics, Mechatronics
- MEMS
- Theoretical and Applied Mechanics
- Dynamical Systems, Control
- Fluid Mechanics
- Engineering Thermodynamics, Heat and Mass Transfer
- Manufacturing Engineering and Smart Manufacturing
- Precision Engineering, Instrumentation, Measurement
- Materials Engineering
- Tribology and Surface Technology

Indexed by SCOPUS, EI Compendex, and INSPEC.

All books published in the series are evaluated by Web of Science for the Conference Proceedings Citation Index (CPCI).

To submit a proposal for a monograph, please check our Springer Tracts in Mechanical Engineering at https://link.springer.com/bookseries/11693.

Krishna Mohan Singh · Sushanta Dutta ·
Sudhakar Subudhi · Nikhil Kumar Singh
Editors

Fluid Mechanics and Fluid Power, Volume 1

Select Proceedings of FMFP 2022

Springer

Editors
Krishna Mohan Singh
Department of Mechanical and Industrial Engineering
IIT Roorkee
Roorkee, Uttarakhand, India

Sushanta Dutta
Department of Mechanical and Industrial Engineering
IIT Roorkee
Roorkee, Uttarakhand, India

Sudhakar Subudhi
Department of Mechanical and Industrial Engineering
IIT Roorkee
Roorkee, Uttarakhand, India

Nikhil Kumar Singh
Department of Mechanical and Industrial Engineering
IIT Roorkee
Roorkee, Uttarakhand, India

ISSN 2195-4356 ISSN 2195-4364 (electronic)
Lecture Notes in Mechanical Engineering
ISBN 978-981-99-7826-7 ISBN 978-981-99-7827-4 (eBook)
https://doi.org/10.1007/978-981-99-7827-4

This Springer imprint is published by the registered company Springer Nature Singapore Pte Ltd.
The registered company address is: 152 Beach Road, #21-01/04 Gateway East, Singapore 189721, Singapore

Paper in this product is recyclable.

Contents

About the Editors

Prof. Krishna Mohan Singh is Professor in the Department of Mechanical and Industrial Engineering at Indian Institute of Technology (IIT) Roorkee. His research interests include the areas of computational mechanics, development of novel parallel algorithms, meshfree methods, shape and topology optimization, fluid dynamics, DNS/LES of turbulent flows, CAE, computer-aided analysis and design of thermo-fluid and multi-physics systems, computational fluid dynamics, modeling and simulation of flow and heat transfer in turbomachines, transport and energy systems.

Prof. Sushanta Dutta is Professor in the Department of Mechanical and Industrial Engineering at Indian Institute of Technology (IIT) Roorkee. His research interests are in the areas of experimental fluid mechanics, experimental heat transfer, optical measurement techniques, active and passive control of flow field, wake dynamics, turbulence study, Schlieren, HWA, PIV, LCT, PSP, microfluidics and heat transfer augmentation using phase change material.

Prof. Sudhakar Subudhi is Professor in the Department of Mechanical and Industrial Engineering at Indian Institute of Technology (IIT) Roorkee. His research interests are in the area of experimental heat transfer and fluid mechanics, heat transfer enhancement of natural and forced convection in water/nanofluids, natural ventilation and unconventional energy systems.

Dr. Nikhil Kumar Singh is Assistant Professor in the Department of Mechanical and Industrial Engineering at Indian Institute of Technology (IIT) Roorkee. His broad research interests include direct numerical simulations of two-phase flows and phase change, computational fluid dynamics and heat transfer, numerical methods and turbulent flows.

Fluid Flow and Heat Transfer

Experimental Modelling to Measure the Seat Leakage in Shutdown System of PFBR

Piyush Kumar Aggarwal, Indranil Banerjee, V. Vinod, and S. Raghupathy

1 Introduction

Prototype Fast Breeder Reactor (PFBR), which is sodium-cooled Fast Breeder Reactor (FBR), has two independent fast-acting and diverse reactor shutdown systems for controlling the power and shutting down the reactor. These are Control and Safety Rod (CSR) shutdown system and Diverse Safety Rod (DSR) shutdown system. CSR shutdown system is used for controlling the reactor power as well as shutting down the reactor, whereas the DSR shutdown system is used only for shutting down the reactor [1]. Nine neutron absorber rods are provided in CSR shutdown system and three neutron absorber rods are provided in DSR shutdown system. In case of Safety Control Rod-Accelerated Movement (SCRAM), the electromagnet gets de-energized in both the shutdown systems. In CSR shutdown system, CSR with lifting mechanism is released, while in DSR shutdown system, mobile DSR alone falls under gravity and finally deposited on their respective dashpot of the subassembly, to shut down the reactor [2]. In case of CSR system failed to act, DSR system is self-sufficient to shut down the reactor. The schematic of the DSR in normal operating condition and deposited condition is shown in Fig. 1. DSR contains Boron Carbide (B_4C) with enrichment of 65% of B-10 isotope, which is a neutron absorber. DSR in the deposited condition absorb neutrons, which are generated due to nuclear fission reaction inside the reactor core. The neutrons absorbed in B-10 result in an (n, α) reaction. This process liberates heat and produces helium gas. The maximum amount of heat that can be generated in DSR is estimated as 1 MWt.

To remove this amount of generated heat, a minimum sodium coolant flow rate of 3 kg/s shall pass through the mobile DSR. The schematic of flow path at this condition is illustrated in Fig. 2. It can be seen from this figure that there are two parallel flow paths: (i) through mobile DSR and (ii) through DSR–dashpot interface.

P. K. Aggarwal (✉) · I. Banerjee · V. Vinod · S. Raghupathy
India Gandhi Centre for Atomic Research, Kalpakkam, Tamil Nadu 603102, India
e-mail: piyushaggarwal786@gmail.com

K. M. Singh et al. (eds.), *Fluid Mechanics and Fluid Power, Volume 1*, Lecture Notes in Mechanical Engineering, https://doi.org/10.1007/978-981-99-7827-4_1

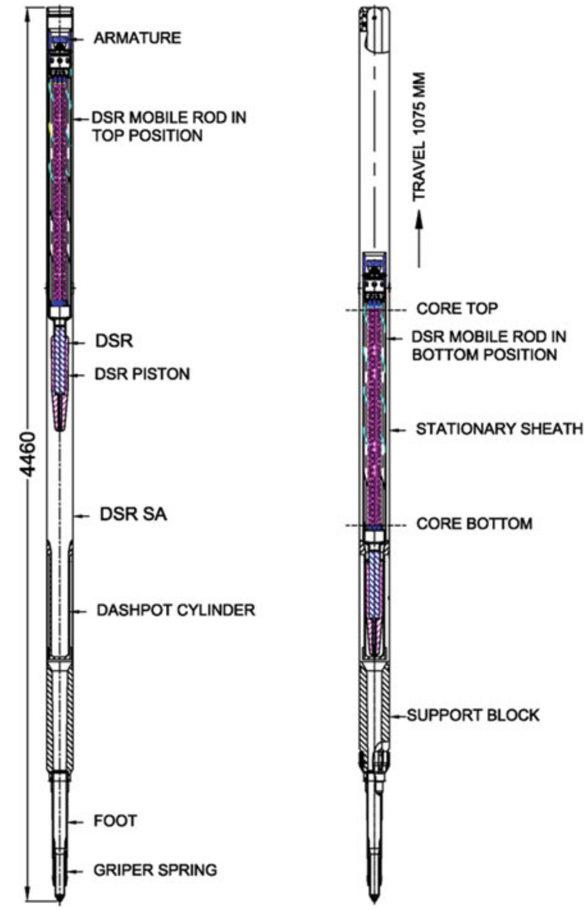

Fig. 1 Schematic of DSR in normal operating condition and deposited condition

The flow between these two parallel paths is apportioned according to their relative hydraulic resistance. Required coolant flow through mobile DSR shall be more than 95% of the total flow and less than 5% of the total flow is allowed to leak through the DSR–dashpot interface.

Therefore, it is required to measure the leakage rate of sodium through DSR–dashpot interface to validate the design. However, carrying out the studies in sodium is costly, time-consuming and requires complicated safety procedure to be followed. Hence, the studies are carried out using water as working fluid in a geometrically similar model due to the closeness of hydraulic properties of sodium and water. However, these water model studies require careful investigation of similarity criteria to arrive at the appropriate test parameters and extrapolation of experimental results into prototype system. Sometimes experiments can be further simplified by simulating the zone of interest only. The present study has been conducted to measure the

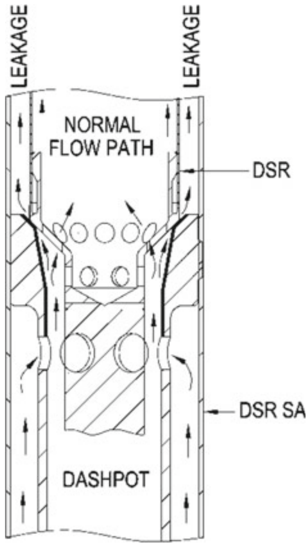

Fig. 2 Schematic of flow path in DSRSA when DSR is deposited on dashpot

leakage rate experimentally through DSR–dashpot interface region by only simulating the geometrical features of interface region. The relation between pressure drop and the seat leakage was developed which will be useful for designing the future DSRSA system.

2 Dimensional Analysis and Similarity Criteria

The total flow rate through DSRSA is apportioned between the DSR mobile assembly and DSR–dashpot seat according to their respective flow path resistance. The pressure loss across the mobile DSR at various operating conditions was measured in earlier water model experiment simulating the full-scale DSRSA. This pressure loss value can be used in a simplified experimental model simulating only the DSR–dashpot region to measure the leakage flow rate. Various forces acting on DSR when it is deposited on dashpot are shown in a schematic diagram shown in Fig. 3. The pressure drop across DSR–dashpot interface which is a metal-to-metal contact surface is function of liquid properties (density and viscosity), surface roughness, geometrical features, velocity of liquid leaking through the seat, and contact pressure as stated in Eq. 1.

$$\Delta P = f(\rho, \mu, \varepsilon, D, V, P_C). \tag{1}$$

The force acting on contact area can be expressed as

$$P_C A_C \mathrm{Sin}\theta = (W - F_B - \Delta P \times A_P). \tag{2}$$

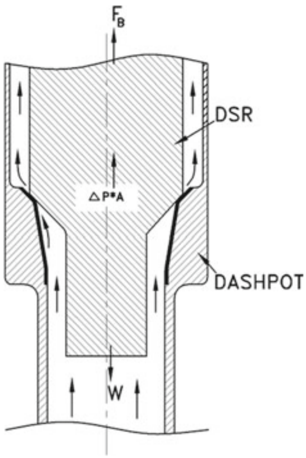

Fig. 3 Schematic diagram of the experimental model

Using dimensional analysis and choosing, ρ, V, and D as repeating variables, following non-dimensional numbers can be formed:

(1) Euler number: $\mathrm{Eu} = \left(\frac{\Delta P}{\rho V^2}\right)$.
(2) Reynolds number: $\mathrm{Re} = \left(\frac{\rho V D}{\mu}\right)$.
(3) Relative surface roughness: $\overline{\varepsilon} = \left(\frac{\varepsilon}{D}\right)$.
(4) Non-dimensional contact pressure: $P_c^* = \left(\frac{P_c}{\rho V^2}\right)$.

Applying Buckingham Pi theorem, it can be written

$$\mathrm{Eu} = f\left(\mathrm{Re}, \overline{\varepsilon}, P_c^*\right). \tag{3}$$

Therefore, in model testing above-mentioned non-dimensional numbers are required to be simulated along with the simulation of geometrical similarity. Calculation of required process parameters in a 1:1 scale water model simulating the DSR–dashpot region and transposition of measured leakage rate through DSR–dashpot interface into reactor condition were carried out using the following procedures:

Step-1: The equivalent differential pressure across the seating interface in the model can be found out from Eu and Re similitudes.

From Eu similitude, it can be written that,

$$\Delta P_m = \left(\frac{\rho_m}{\rho_p}\right) \times \left(\frac{V_m}{V_p}\right)^2 \times \Delta P_p. \tag{4}$$

*The Subscript '*m*' is used for model and '*p*' is used for prototype.

From Re similitude, it can be written that,

$$\left(\frac{V_m}{V_p}\right) = \left(\frac{\rho_p}{\rho_m}\right) \times \left(\frac{\mu_m}{\mu_p}\right). \quad (5)$$

The equivalent differential pressure in model across DSR–dashpot interface at nominal leakage rate in reactor can be estimated from Eq. 6 which is deduced by combining Eqs. 4 and 5.

$$\Delta P_m = \left(\frac{\rho_p}{\rho_m}\right) \times \left(\frac{\mu_m}{\mu_p}\right)^2 \times \Delta P_p. \quad (6)$$

Differential pressure across DSR–dashpot interface in reactor (ΔP_P) is equal to the pressure drop across mobile DSR assembly when DSR is deposited on dashpot. This is because these are two parallel flow paths. In earlier experiment, the pressure drop across mobile DSR in reactor at nominal flow rate of 3.18 kg/s was estimated for the following two cases:

Case 1: $\Delta P_P = 5.58$ kPa, when DSR is deposited on dashpot and the lifting mechanism for DSR is at the top most position, not attached to DSR.

Case 2: $\Delta P_P = 7.6$ kPa, when DSR is deposited on dashpot and the lifting mechanism for DSR is engaged with the DSR, prior to lifting it.

These values are used to estimate the differential pressure requirement across the seating interface in the model.

Step-2: The contact pressure at seat in the model shall be equal to the contact pressure of prototype.

$$(P_c)_m = (P_c)_p. \quad (7)$$

$(P_c)_p$, which is contact pressure at DSR–dashpot interface in prototype, can be estimated using Eq. 2.

$$(P_C)_P = \frac{1}{(A_c)_p \mathrm{Sin}\theta}\{(W - F_B - A_P \times \Delta P)\times\}_p,$$

where

$A_P = 9.33 \times 10^{-3}$ m^2 (contact diameter is 109 mm).

$A_C = 1.712 \times 10^{-3}$ m^2 (lateral contact width 5 mm).

$\theta = 45°$.

$W_B = W - F_B = 45 \times 9.81$ kg m/s^2 (apparent wt. in sodium at 400 °C).

The values of contact pressure for the above-mentioned two cases are as follows:

(a) For case 1, $\Delta P_P = 5.58$ kPa,

$$(P_C)_P = \frac{1}{1.712 \times 10^{-3} \times 0.707}\left\{(45 \times 9.81) - 9.33 \times 10^{-3} \times 5.58 \times 10^3\right\}$$
$$= 321.7\,\text{kPa}$$

(b) For case 2, $\Delta P_P = 7.6$ kPa,

$$
\begin{aligned}
(P_{\mathrm{C}})_{\mathrm{P}} &= \frac{1}{1.712 \times 10^{-3} \times 0.707}\left\{(45 \times 9.81) - 9.33 \times 10^{-3} \times 7.6 \times 10^{3}\right\} \\
&= 306.1\,\mathrm{kPa}
\end{aligned}
$$

To maintain the equivalent contact pressure in model as found out using Eq. 7, the equivalent weight of DSR in model can be estimated from the following equation:

$$
(P_{\mathrm{c}})_{\mathrm{m}} = \frac{1}{(A_{\mathrm{c}})_{\mathrm{m}} \times \mathrm{Sin}45^{\circ}}\{(W - F_{\mathrm{B}} - A_{\mathrm{P}} \times \Delta P)\}_{\mathrm{m}}, \tag{8}
$$

$$
(W - F_{\mathrm{B}})_{\mathrm{m}} = \left[(P_{\mathrm{C}} \times A_{\mathrm{C}}) \sin 45^{\circ} + (\Delta P)(A_{\mathrm{P}})\right]_{\mathrm{m}}. \tag{9}
$$

In the present experimental setup, only DSR–dashpot region is simulated in the model and full DSR is not simulated. A small portion of the DSR foot is immersed in water, and hence, the buoyancy force acting on the model is neglected. Therefore, Eq. 9 can be modified as follows:

$$
W_{\mathrm{m}} = [0.707 \times (P_{\mathrm{C}})(A_{\mathrm{C}}) + (\Delta P)(A_{\mathrm{P}})]_{\mathrm{m}}. \tag{10}
$$

Step-3: The leakage mass flow rate in the model ($\dot{m}_{\mathrm{m}}$) can be measured for differential pressure (ΔP_{m}) across seating interface. The flow through the narrow gap of DSR seating on dashpot is expected to be viscous dominant. Therefore, viscous forces and inertial forces will be characterizing the leakage flow through seating. Hence, the leakage mass flow rate can be extrapolated to reactor condition using Re similitude shown in the following equation:

$$
\dot{m}_{\mathrm{p}} = \rho_{\mathrm{p}} \times V_{\mathrm{p}} \times A_{\mathrm{p}}.
$$

Also using Eq. 5,

$$
V_{\mathrm{p}} = \left(\frac{\rho_{\mathrm{m}}}{\rho_{\mathrm{p}}}\right) \times \left(\frac{\mu_{\mathrm{p}}}{\mu_{\mathrm{m}}}\right) V_{\mathrm{m}}
$$

$$
\dot{m}_{\mathrm{p}} = \rho_{\mathrm{p}}\left(\frac{\rho_{\mathrm{m}}}{\rho_{\mathrm{p}}}\right) \times \left(\frac{\mu_{\mathrm{p}}}{\mu_{\mathrm{m}}}\right) \times V_{\mathrm{m}} \times A_{\mathrm{p}} = \left(\frac{\mu_{\mathrm{p}}}{\mu_{\mathrm{m}}}\right) \times \dot{m}_{\mathrm{m}}. \tag{11}
$$

Density and dynamic viscosity of water at 55 °C and sodium at 400 °C are tabulated in Table 1. These values are considered for estimation of the required value of ΔP_{m}, $(P_C)_{\mathrm{m}}$, and $(W)_m$ by using Eqs. 6, 7, and 10 and tabulated in Table 2.

Table 1 Hydraulic properties of water and sodium for test conditions

	Dynamic viscosity (kg/m-s)	Density, (kg/m^3)
Water at 55 °C	0.50×10^{-3}	986
Sodium at 400 °C	0.281×10^{-3}	857

Table 2 Equivalent pressure drop and required weight of DSR in model for different test conditions

Test conditions using water at 55 °C	ΔP_m (kPa)	$(P_c)_m$ (kPa)	$(W)_m$ (kg)
Case 1: $\Delta P_p = 5.58$ kPa	15.35	321.7	54.3
Case 2: $\Delta P_p = 7.6$ kPa	20.91	306.1	57.6

3 Description of Experimental Model and Methodology

A 1:1 scale simplified model of DSR–dashpot interface has been fabricated to conduct the experimental leakage rate measurements in water. The apparent weight of actual DSR in sodium at 400 °C is 45 kg in PFBR. The DSR–dashpot leakage measurement testing is conducted by maintaining the same apparent weight of DSR as in prototype, which is 45 kg, instead of 54.3 kg estimated weight for model testing mentioned in Table 2. However, the differential pressure (ΔP_m) across the seating interface was simulated as per Table 2. The less simulated weight of mobile DSR will give less sitting pressure in water testing compared to the prototype for simulated differential pressure across the seating interface. Since, additional wt. will further reduce the leakage and this weight will provide conservative measurement of leakage flow. Leakage flow was measured at various differential pressures across DSR–dashpot interface. In model test setup, DSR weight is simulated with a solid rod. The seating portion of DSR–dashpot interface is fabricated exactly same as in PFBR DSR–dashpot seating interface profile with same hard-facing material. The schematic of fabricated DSR and dashpot is shown in Fig. 4.

The schematic of experimental test setup is shown in Fig. 5.

A water tank of 1.75 m^3 was used to maintain the leakage flow. An immersion-type, rod heater was used to raise the water temperature. Temperature of water was monitored continuously. To achieve the desired flow rate and hence differential pressured, compressed air was used to increase the pressure inside the tank. A pressure transmitter (PT) was provided to measure the gauge pressure at the entry to DSR–dashpot interface. Tape heaters and insulation were provided on the connecting pipe between test setup and tank to maintain the constant water temperature.

The photographic view is shown in Fig. 6. The experiment was conducted at water temperature of 55–60 °C. Filtered water was used during the experiment, and suspended particle of size < 10 micron was expected after filtration. Subsequent to this, the water tank was pressurized using compressed air. A pressure transmitter was connected at dashpot to measure gauge pressure inside the dashpot. Differential pressure across DSR–dashpot is equal to the measured gauge pressure since the dashpot outlet is open to atmosphere. Leakage flow rate was measured by water

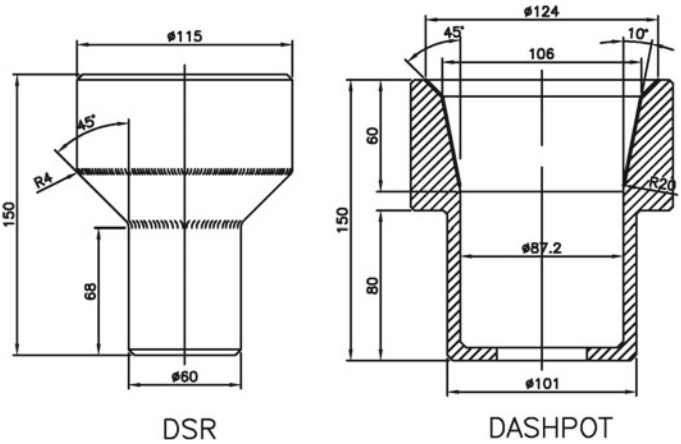

Fig. 4 DSR–dashpot interface in model

Fig. 5 Schematic of the experimental setup

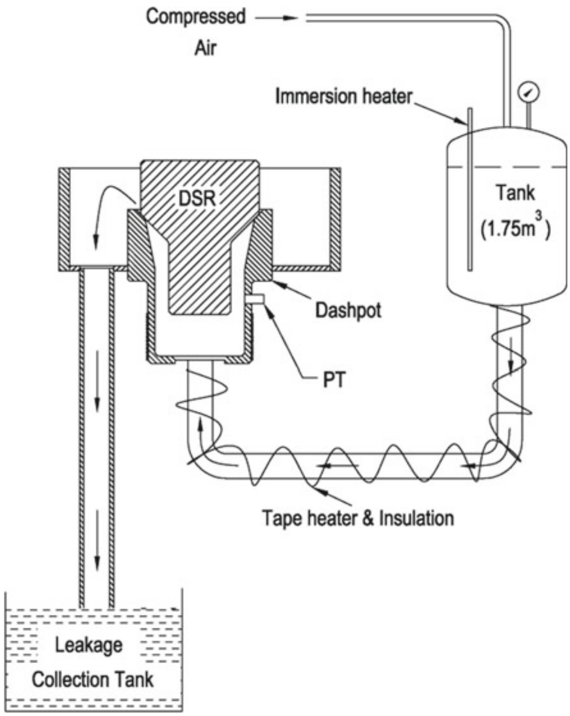

Fig. 6 Photographic view of the experimental setup

volume collection method. The leakage flow rate was measured at different differential pressure conditions. Experimental leakage measurement tests were conducted with random alignment of the DSR sitting on dashpot.

4 Results and Discussions

Measurement of leakage rate has been carried out for a wide range of differential pressure across DSR–dashpot interface. The plot for differential pressure across DSR–dashpot interface versus leakage mass flow rate of water is presented in Fig. 7.

It can be seen from the above figure that the leakage rate is a strong function of the DSR orientation inside dashpot. Even a minor change in DSR sitting orientation on dashpot can alter the leakage rate significantly. There is a contact between DSR and dashpot interface, which is not allowing the DSR to tilt significantly. However, during free seating of DSR on dashpot at different orientations, minor tilting of DSR happens, which breaks the surface contact at interface and significant leakage happens. Therefore, DSR is lifted manually, rotated, and positioned freely number of times in its seat on dashpot to get the maximum leakage. The legend corresponding to Test-2 in Fig. 7 shows the upper bound of the leakage flow rate.

All the experimental data have been transposed to reactor condition using the similitude laws as discussed in previous section. The sodium leak rate (g/s) vs. differential pressure across DSR–Dashpot interface for reactor conditions is shown in Fig. 8. The upper bound characteristic is also plotted in this figure to estimate the maximum possible leakage rate. It can be seen from this figure that the maximum sodium leakage rate considering the upper bound curve fit equation for case—1 ($\Delta P = 5.58$ kPa) is 15 g/s which is around 0.5% of the total flow rate (3.18 kg/s) through DSRSA, and for case—2 ($\Delta P = 7.6$ kPa), the maximum leakage rate is found to be

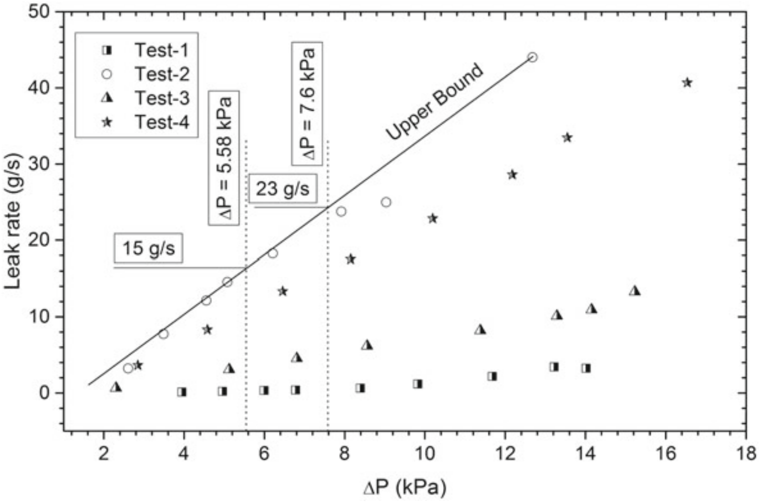

Fig. 7 Water leakage across DSR–dashpot seating with varying differential pressures

23 g/s which is 0.72% of the rated flow rate. These leakage rates are much lower than the maximum allowable limit of leakage flow through DSR–dashpot interface which is 5% of the nominal flow rate through DSRSA in reactor.

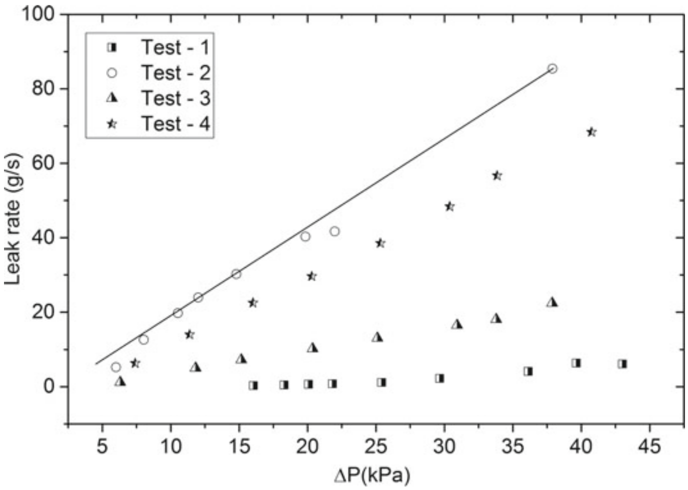

Fig. 8 Leakage rate versus pressure drop across DSR–dashpot

5 Conclusion

A study has been carried out to estimate the leakage rate through DSR–dashpot interface when DSR is deposited on the dashpot. The pressure drop in test model has been simulated using Eu and Re numbers. A correlation has been derived to estimate the weight of DSR in testing condition, to generate the same amount of contact pressure on the seat as in PFBR. It was observed from the experiment that even slight change on the sitting orientation of DSR can alter the leakage rate significantly. Thus, DSR is positioned at different orientations and water leakage rate has been measured. The experimental measurement has been carried out with water at higher temperature. All the experimental measurement data were transposed using appropriate similitude laws. An upper bound characteristic curve is also established. Since the data scatter is very high due to orientation of DSR inside dashpot, an uncertainty analysis was also carried out. The estimated maximum sodium leakage rate through DSR–dashpot interface at pressure drop of 5.58 kPa (corresponding to the situation of DSR sitting on dashpot just after shutdown) is found to be 21.5 g/s which is only 0.7% of nominal flow rate (3.18 kg/s). Subsequently, the sodium leakage was also estimated for other condition which represents the situation of DSR deposited in dashpot and lifting mechanism is attached with it. As mentioned earlier, the corresponding pressure drop across DSR–dashpot interface is 7.6 kPa. At this pressure drop, maximum leakage rate is found to be 32.9 g/s which is 1.03% of the rated flow rate. These leakage rates are much lower than the allowable limit of 5% of the nominal flow rate through DSRSA in reactor.

Nomenclature

W	Weight of the mobile DSR [kg]
F_B	Buoyancy force acting on mobile DSR due to full submergence in sodium [kg m/s^2]
W_A	Apparent weight [kg]
A_P	Projected area of DSR m^2
A_C	Contact area of the lateral contact surface m^2
ΔP	Pressure drop across DSR–dashpot interface (seating) N/m^2
θ	Angle of inclined contact surface degree
ρ	Density of the liquid [kg/m^3]
μ	Dynamic viscosity of the liquid kg/m-s
ε	Roughness of the contact surface mm
D	Characteristic length representing geometrical features m
V	Velocity of leakage flow m/s
P_C	Contact pressure at DSR–dashpot interface N/m^2

References

1. Vijayashree R et al (2010) Design, development, testing and qualification of diverse safety rod and its drive mechanism for a prototype fast breeder reactor. J Eng Gas Turbines Power 132(10)
2. Nimala Sundaran M et al (2017) Experimental seismic qualification of diverse safety rod and its drive mechanism of prototype fast breeder reactor. In: International conference on fast reactors and related fuel cycles: next generation nuclear systems for sustainable development, IAEA, Vienna (Austria), FR17, June 2017

Performance of Water-Based Loop Heat Pipe at Different Ambient Conditions for Thermal Management in Terrestrial Applications

Shail N. Shah, Fagun A. Pithadiya, and Sanjay V. Jain

1 Introduction

The twenty-first century has seen a rise in the importance of thermal management issues in several industrial applications. Due to miniaturization and an increase in heat-generating equipment, various industries including the space industry, electronics, mobile, laptop, supercomputers, etc., are experiencing problems with thermal management. Loop heat pipes absorb heat from the heated surface, converting the working fluid to vapor as a result. LHP has a wick structure to enable fluid flow back to the evaporator in a variety of orientations. LHP was developed first time in 1972 at the Ural Polytechnical Institute of Thermal Physics by Maydanik et al. [1]. They tested an LHP with a length of 1.2 m and a capacity of around 1 kW.

Conventional heat pipe (HP) consists of single evaporator and condenser section and the primary wick. The addition of secondary wick and C.C. in LHP is the primary structural change between HP and LHP. Transport lines in LHP separate the heat source from the heat sink, increasing LHP's flexibility. Insufficient liquid in the primary wick causes a dry-out condition. In this situation, the pressure differential between the C.C. and the evaporator causes liquid to flow from the C.C. through the secondary wick to the evaporator section and then to the primary wick, allowing the LHP to absorb more heat from the heat source as shown in Fig. 1.

Conventional heat pipes have significant length and dry-out constraints, whereas LHP can operate at larger heat loads and over longer distances between the evaporator and condenser portions. Nakamura et al. [2] investigated long-distance heat transfer for heat loads of 1000 W and up to 10 m length.

Water-based LHP can be used for terrestrial applications like thermal management in mobile, laptop, defense, air conditioning. Ambient condition has significant effect

S. N. Shah · F. A. Pithadiya · S. V. Jain (✉)
Department of Mechanical Engineering, Institute of Technology, Nirma University, Ahmedabad, India
e-mail: sanjay.jain@nirmauni.ac.in

K. M. Singh et al. (eds.), *Fluid Mechanics and Fluid Power, Volume 1*, Lecture Notes in Mechanical Engineering, https://doi.org/10.1007/978-981-99-7827-4_2

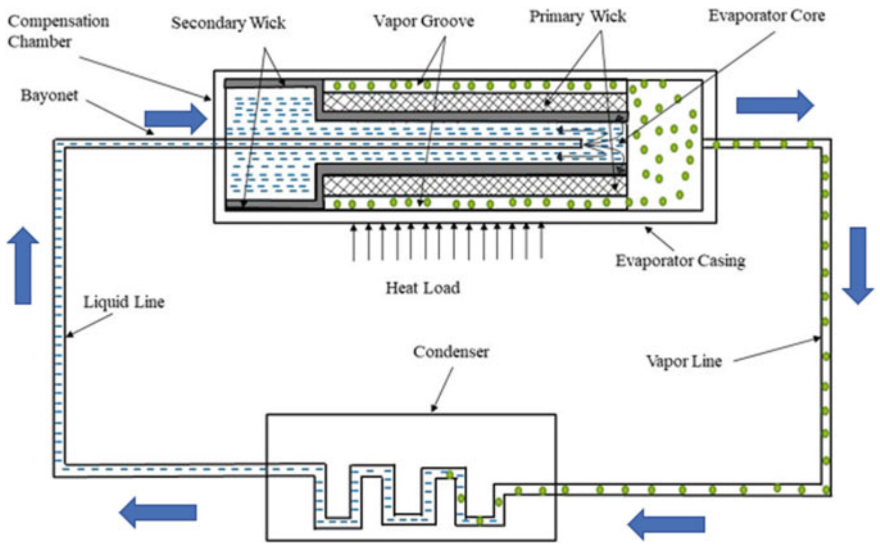

Fig. 1 Schematic diagram of LHP

on the performance of LHP as it will vary heat exchange and overall loop temperature based on the amount of heat load to be removed from the source.

2 Literature Review and Objective

Mathematical modeling of LHP has been done over the years in two segments: single-phase analysis and two-phase analysis. Single-phase analysis of LHP was done in initial years for mathematical modeling to understand the working of LHP by Kaya et al. [3]. Later, Hoang et al. [4] developed first two-phase analysis model of ammonia-based LHP for space application. Water-based LHP for terrestrial application is under immense research since last half decade. Flat-plate LHP was developed by Tsai et al. [5] for better gripping on electronic components and better heat transfer. It was found to be less efficient than conventional LHP, but better flexibility was obtained for mounting. Singh et al. [6] analyzed water-based miniature LHP (mLHP) for computer CPU cooling. It was concluded that a mLHP can be employed to thermally regulate electronic devices with small footprints and high heat flux chipsets. Vasiliev et al. [7] analyzed use of LHP for high-power electronic components. It was discovered that the vapor groove fabrication affects the mean pore diameter and wick porosity on the surface of vapor removal grooves. LHP for server cooling was analyzed by Maydanik et al. [8]. Various condenser cooling techniques were tested using miniature ammonia LHPs and a CPU thermal simulator. Choi et al. [9] analyzed water-based LHP for electronic cooling with sintered porous wick. Hu et al. [10] developed 3D-printed wick and performance of LHP was found to be in line with sintered wick structure. In order to explain the two-phase heat transfer coefficient and pressure decrease in depth, Adoni et al. [11] created a steady-state model using the energy and mass conservation equations. Different structural modifications have been carried out over the years to meet customer requirement as well as to improve performance of LHP [12–14]. Micro and miniature LHPs have been developed to meet miniature cooling requirement for terrestrial applications [15, 16].

The performance of LHP is significantly impacted by the environment. The literature study revealed that only a small number of researchers have thoroughly investigated the combined effects of ambient condition on various LHP characteristics. Novelty of the present work is the combined analysis of water-based LHP for effect of ambient conditions (i.e., 10, 22, and 40 °C) on the parameters like steady-state operating temperature (SSOT), condenser outlet temperature (T_{co}), liquid line outlet temperature (T_{lo}), two-phase pressure drop across condenser (i.e., $\Delta P_{2\phi}$), heat exchange from compensation chamber (C.C.), and liquid line to ambient (i.e., $Q_{\text{c.c.-amb}}$, $Q_{\text{L.L.-amb}}$) and resistance of LHP (R_{LHP}).

3 Mathematical Modeling of Loop Heat Pipe

In the present study, to analyze performance of loop heat pipe with water as a working fluid, several dimensional parameters were taken from the literature for the validation purpose as mentioned in Table 1.

The total heat load (Q_{l}) distribution in the system is the addition of evaporator heat transfer (Q_{evap}), heat leak from evaporator compensation chamber (Q_{Heatleak}), heat transfer from compensation chamber to ambient, and heat transfer from liquid line to ambient as per Eq. (1).

$$Q_{\text{l}} = Q_{\text{evap}} + Q_{\text{Heatleak}} + Q_{\text{L.L.-amb}} + Q_{\text{c.c.-amb}}. \tag{1}$$

Table 1 LHP dimensional parameters

Component	Dimension (OD/ID length)	Unit
Evaporator	Φ 42/32 × 100	mm
C.C	Φ 42/32 × 100	mm
Vapor line	Φ 6/4 × 220	mm
Liquid line	Φ 6/4 × 150	mm
Condenser	Φ 6/4 × 300	mm
Wick	Φ 30/20 × 100	mm
Porosity	30.9	%
Pore radius	54	μm

Evaporator wall temperature (T_{evp}) can be calculated as per Eq. (2) from the natural convection phenomenon.

$$T_{\text{evp}} = T_{\text{amb}} + \frac{Q_1}{h_{\text{air}}A}. \tag{2}$$

Temperature of vapor (T_{h}) at evaporator section was calculated using Eq. (3).

$$T_{\text{h}} = T_{\text{evp}} - \left(T_{\text{evp}} - T_{\text{evpsat}}\right)e^{\left(\frac{-h_{\text{evp}}A\Delta L}{mCpL}\right)}, \tag{3}$$

where A is evaporator wall area (m^2).

Liquid line outlet temperature (T_{lo}) was found using Eq. (4) by applying resistance method.

$$T_{\text{lo}} = T_{\text{amb}} + (T_{\text{co}} - T_{\text{amb}})e^{\left(\frac{-L}{mRCp}\right)}. \tag{4}$$

Two-phase analysis along the condenser section was done using Lockhart methodology [4]. For the analysis, Eqs. (5–7) were used.

$$\Delta P_{2\Phi} = \int_{x_{\text{out}}}^{x_{\text{in}}} \frac{\Phi_1^2 f_1(1-x)^2}{2D\rho_1}\left(\frac{m}{A}\right)^2\left[\frac{\text{d}z}{\text{d}x}\right]\text{d}x, \tag{5}$$

$$\Phi_1 = \left[1 + \left[\frac{C}{X}\right] + \left[\frac{1}{X^2}\right]\right], \tag{6}$$

$$X = \left[\frac{f_1}{f_{\text{g}}}\right]^{0.5}\left[\frac{\rho_{\text{g}}}{\rho_1}\right]^{0.5}\left[\frac{1-x}{x}\right]. \tag{7}$$

Resistance of loop heat pipe (R_{LHP}) was calculated using Eq. (8).

$$R_{\text{LHP}} = \frac{T_{\text{evp}} - \frac{(T_{\text{cc}}+T_{\text{co}})}{2}}{Q_1}. \tag{8}$$

Single-phase pressure drop in vapor line and liquid line was calculated using Eq. (9) and pressure drop in wick structure was found using Eq. (10).

$$\Delta P = \left(\frac{8\mu mL}{\pi\rho r^4}\right), \tag{9}$$

$$\Delta P_{\text{w}} = \frac{\mu m \ln\left(\frac{D_{\text{ow}}}{D_{\text{iw}}}\right)}{2\pi\rho L_{\text{wick}}K_{\text{wick}}}. \tag{10}$$